Korean J. Chem. Eng., 39(9), 2394-2404 (2022)
DOI: 10.1007/s11814-022-1100-9

pISSN: 0256-1115
eISSN: 1975-7220

Activated carbon (AC)-metal-organic framework (MOF) composite: Synthesis, characterization and dye removal

Sina Soroush*,, Niyaz Mohammad Mahmoodi*,†, Bayramali Mohammadnezhad**, and Abdolreza Karimi****

*Department of Environmental Research, Institute for Color Science and Technology, Tehran, Iran
**Department of Civil Engineering, Qom University of Technology (QUT), Qom, Iran
(*Received 10 November 2021 • Revised 29 January 2022 • Accepted 4 March 2022*)

Abstract−Activated carbon (AC), one of the most common adsorbents, and metal-organic framework (MOF), an interesting class of materials, were used for synthesizing AC/MOF composite by the solvothermal method. The strategy designed in this paper is to improve the removal and adsorption performance of AC for dye. MIL-53(Fe) was synthesized on the commercial activated carbon (CAC) to prepare CAC/MIL-53(Fe) composite. Direct Red 23 (DR23) anionic dye was used as a model contaminant. FT-IR, XRD, SEM, and EDX analyses were applied to study the structure and characteristics of CAC/MIL-53(Fe). The parameters (the solution pH, amount of adsorbent dosage, initial dye concentration, and contact time) affecting the dye removal efficiency were investigated. The percentage of dye removal (DR23) under optimal conditions by commercial activated carbon and CAC/MIL-53(Fe) was 50% and 99.9%, respectively. The maximal capacity of adsorption was also raised from 50 to 100 mg/g. The adsorption isotherm and kinetics followed the Langmuir and pseudo-second-order models, respectively.

Keywords: CAC/MIL-53(Fe) Composite, Metal-organic Framework, Commercial Activated Carbon (CAC), Dye Removal

INTRODUCTION

The textile dyeing industry is a significant polluter of the environment due to the massive discharge of wastewater containing various dyes. According to statistics, around 1.6 million tons of dyes are produced each year, with 10-15 percent discarded as wastewater. Water in which even small quantities of dye have been added is noticeable and unwanted. The poor biodegradability of dyes causes them to be more resistant to conventional water treatment methods. As a consequence, the removal of these kinds of dyes from wastewater before their release is a critical study issue from an environmental and safety standpoint. To remove dyes from contaminated wastewater, a variety of treatment procedures have been used, including biological processes, adsorption, catalysis, ozonation, and electrochemical. Among these techniques, adsorption is the best known for its ease of operation, low cost, speed, high efficiency, and environmental friendliness [1-8].

Commercial activated carbon (CAC) has long been regarded as one of the most popular and extensively utilized adsorbents in water and wastewater treatment [9]. The most promising option for textile wastewater treatment has been identified as CAC with a high specific surface area and porosity [10].

One creative approach for optimizing the adsorption process is to synthesize composite materials with novel adsorption characteristics based on the collective behavior of the composite's constituent sorbents [11].

Metal-organic frameworks (MOFs) are highly organized porous crystalline composite materials that include metal clusters and multifunctional organic linkers and are recognized as coordination polymers. Yaghi and Li were the first in developing MOFs with persistent porosity in 1995 [12]. MOFs are appealing to researchers working on creating next-generation adsorbents because of their varied nature and remarkable characteristics. They have emerged as valuable materials with exploitable properties, such as tunable ultrahigh porosity, crystalline nature, changeable structure, versatile functionality, huge surface area and pore volumes, uniform pore size, particular interaction sites for a selected adsorbate, superior optoelectronic properties, and excellent mechanical and thermal stability [13,14]. MOFs have been employed for a variety of industrial applications, such as adsorption [15,16], sensing [17], separation [18,19], catalysis [20], and proton conduction [21], also in some emerging technologies, such as light-harvesting [22], photocatalysis [23], drug delivery [24], nanofluids [25], and biocatalysts [26], due to their prominent structural properties. They are classified into many types, including UiOs (University of Oslo), MILs (Material of Institute Lavoisier), and ZIFs (Zeolitic Imidazolate Frameworks). One of the most significant types of MOF is MILs. Among the many kinds of MILs, MIL-53(Fe) as an iron-based MOF is extensively utilized for dye removal owing to multiple characteristics such as low cost, stability in diverse reaction conditions, extremely low toxicity, and even non-toxicity. Furthermore, the Fe^{3+} metal ion with a high valence can be combined with carboxylate-type ligands to form a water-stable MOF [27]. MIL-53(Fe) was suggested owing to its many characteristics, such as inexpensive cost, stability in diverse reaction conditions, extremely low toxicity, and even non-toxicity [28].

A literature indicated that CAC/MIL-53(Fe) was used to remove dye. Herein, CAC/MIL-53(Fe) was synthesized and utilized to remove anionic dye (Direct Red 23: DR23) from water. In addi-

†To whom correspondence should be addressed.
E-mail: mahmoodi@icrc.ac.ir

tion, the parameters (the pH of the solution, amount of adsorbent dosage, initial dye concentration, contact time) affecting the adsorption process and DR23 removal were investigated. Also, the isotherm and kinetics of adsorption and reusability were investigated.

MATERIALS AND METHODS

1. Materials

Commercial activated carbon, iron (III) chloride hexahydrate ($FeCl_3 \cdot 6H_2O$), 1,4-benzene dicarboxylic acid (Terephthalic acid, $C_8H_6O_4$), and *N, N*-dimethyl formamide (DMF, C_3H_7NO) were applied to synthesize MIL-53(Fe) and composite. Methanol was also used to wash the resulting precipitate in the synthesis procedure of MIL-53(Fe), and CAC/MOF composites and ethanol were also used in reusability. Direct Red 23 (DR23) was used as an organic dye and pollutant model. In addition, sodium hydroxide (NaOH) and hydrochloric acid (HCl) were utilized to adjust the pH of the solution. The chemicals and solvents were obtained from Merck (Germany).

2. Synthesis of MIL-53(Fe)

The solvothermal method was used to synthesize MIL-53(FE). The molar ratio of $FeCl_3 \cdot 6H_2O$, terephthalic acid (H_2BDC), *N, N* dimethylformamide (DMF) is 1 : 1 : 280 (0.674 g, 0.415 g, 56 mL, respectively) [29]. This mixture was stirred for 30 min at room temperature (25 °C). Following the sonication, the resultant mixture was left to sit in the bath for 15 min. The resultant solution was placed in a Teflon-lined steel autoclave after it had been sonicated. It was heated for 15 h at 150 °C and then allowed to cool before cutting. To separate the DMF solution from the resultant combination, the mixture was centrifuged in the following step (at 6,000 rpm). A pale brown powder was created, and the final product was washed with methanol [28]. Finally, the powder was heated for 15 h at 150 °C in an oven.

3. Synthesis of CAC/MIL-53(Fe)

For synthesis of CAC/MIL-53(Fe), in the presence of AC, the MIL-53(Fe) in situ was used. 1 g powdered CAC was added to the 20 mL of *N, N*-dimethylformamide (DMF). This mixture was sonicated for 15 min. After that, the mentioned values were used in the synthesis of MIL-53(Fe) with the CAC solution and vigorously stirred at room temperature (25 °C) for 30 min. The mixture was sonicated (in a bath) for 30 min. Following the sonication process, the mixture was put in an autoclave. It was heated for 15 h at 150 °C. The resulting product was washed and centrifuged, and drying steps were performed similarly in the synthesis process of MIL-53(Fe). For the synthesis of CAC/MIL-53(Fe) the ratio (1 : 0.3) of CAC to MOF was used.

4. Materials Characterization

The crystallographic properties of the synthesized materials were determined using X-ray diffraction (XRD) analysis. The PANalytical Crystal Netherlands X-ray diffractometer was used to evaluate the samples. The produced adsorbent surface texture morphology was investigated using LEO 1455VP scanning electron microscopy (SEM). The TESCAN-MIRA III was used to evaluate the produced adsorbent's energy-dispersive X-ray (EDX). The Perkin Elmer analyzer was used to assess the sample using the various functional groups of the obtained Fourier transform infrared (FT-IR) spectrum.

5. Experimental Batch Adsorption

In this study, to appraise the efficiency of the synthesized adsorbent, the dye solution was prepared in a 100 mL container with a concentration of 20 mg/L at pH=3, which HCl and NaOH was adjusted. Then different quantities of adsorbent dosage (0.005, 0.01, 0.015, and 0.02 g) for dye adsorption were evaluated as the initial dosage of adsorbent in 90 min at room temperature. The dye solution was sampled every 15 min by separating the adsorbent particles through centrifuging. Dye adsorption was measured using a UV-Vis spectrophotometer at λ_{max} of Direct Red 23 (503 nm). The amount of adsorbent dosage, which had the highest dye removal (%), was the optimal dosage considered. The factors affecting adsorption (the pH, initial dye concentration, and contact time) were investigated at room temperature. The reusability of the composite was also tested.

The percentage of dye removal (R%) and the quantity of dye adsorption at equilibrium (q_e) were calculated using Eqs. (1) and (2), respectively [30].

$$R\% = \frac{(C_0 - C_t)}{C_0} \times 100 \quad (1)$$

$$q_e = \frac{(C_0 - C_e)V}{M} \quad (2)$$

The dye concentrations at t=0 and t (mg/L) are C_0 and C_t, respectively. V and M represent the volume of the dye solution (L) and the weight of the adsorbent (g), respectively [31].

RESULTS AND DISCUSSION

1. Characterization

1-1. XRD Analysis

In Fig. 1, the crystallographic patterns of the synthesized samples were ascertained by XRD analysis. The diffraction pattern of CAC in Fig. 1 is shown as amorphous material and does not indicate the presence of crystalline phases. The XRD diffraction pattern observed for MIL-53(Fe) synthesized in this investigation was

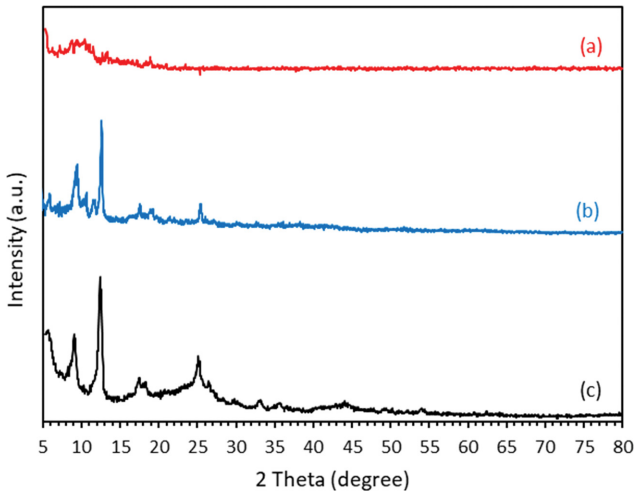

Fig. 1. XRD pattern of the samples (a) CAC, (b) MIL-53(Fe), and (c) CAC/MIL-53(Fe).

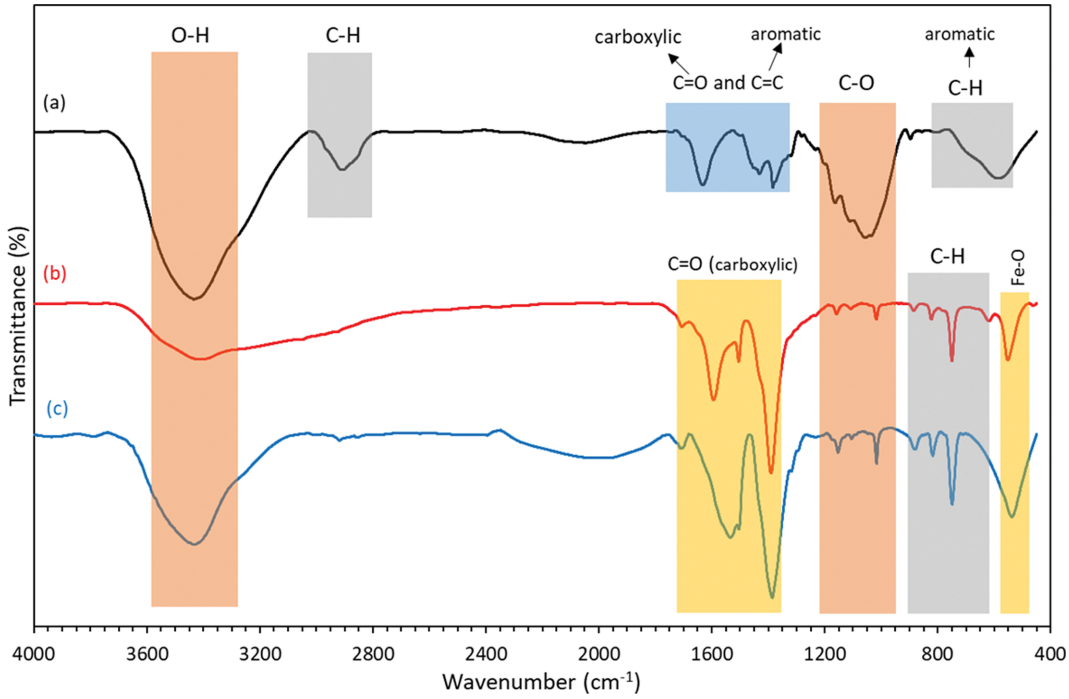

Fig. 2. FTIR spectrum of the samples (a) CAC, (b) MIL-53(Fe), and (c) CAC/MIL-53(Fe).

in satisfactory agreement with the XRD diffraction pattern of this MOF available in the published literature [32-34]. Thus, the MIL-53(Fe) MOF was successfully synthesized [35]. The composite depicts the main diffraction peaks in MIL-53(Fe) (2θ=9.42°, 12.6°, 17.51°, and 25.39°). As shown, the crystal structure of MIL-53(Fe) is preserved after combining MIL-53(Fe) with CAC.

1-2. FT-IR Analysis

FT-IR spectroscopy is based on the idea that molecules adsorb certain wavelengths of infrared light preferentially, resulting in vibrational and rotational state changes. FT-IR spectroscopy provides valuable information on molecule structure [36]. Fig. 2(a) shows the CAC spectrum. The functional group represents the bands between 3,200 and 3,450 cm^{-1}, which is related to the hydroxyl group's O-H stretching vibration, and the peaks at a range of 2,800-3,000 cm^{-1} were assigned to aliphatic C-H stretching [37]. The C=O of the carboxylic group comes at 1,540-1,750 cm^{-1}, and the aromatic C=C group is at 1,600-1,450 cm^{-1} [38]. The range 1,250-1,384 cm^{-1} is assigned to phenolic O-H bending in CAC [39]. The bands at 1,000-1,200 cm^{-1} correspond to C-O stretching in alcohols and phenols [40], and the peak at 586 cm^{-1} represents aromatic C-H bending vibrations. As shown in Fig. 2 (spectrum (b) and (c)), the results of the FTIR spectrum of MIL-53(Fe) are quite identical to those of the CAC/MIL-53(Fe). The characteristic peaks of MIL-53(Fe) for MIL-53(Fe) and O-H (stretching vibration, 3,430 cm^{-1}) were detected in the range 1,400-1,700 cm^{-1}. The adsorption band observed at 1,550 cm^{-1} in each group is related to carboxyl ligand groups coordinated with metal centers [26]. The peak at 750 cm^{-1} is related to the bending vibrations of C-H of benzene rings [27]. The presence of (Fe-O) at 537 cm^{-1} indicates the creation of a metal-oxo link between the carboxylic group of terephthalic acid and Fe (III) for CAC/MIL-53(Fe) [28]. Hence, from the FT-IR spectra out-

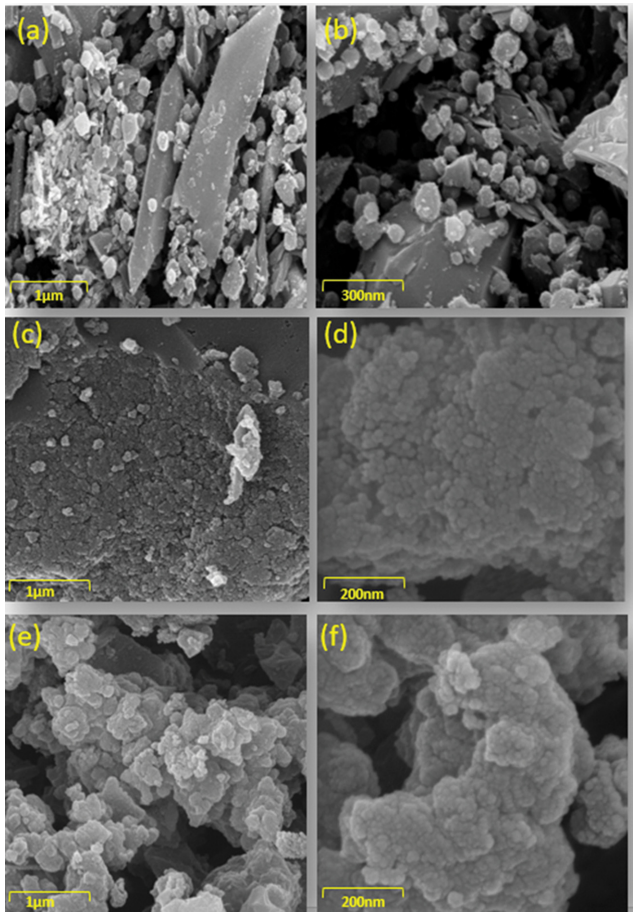

Fig. 3. SEM images of the samples: (a), (b) MIL-53(Fe), (c), (d) CAC, and (e), (f) CAC/MIL-53(Fe).

comes, it is evident that the structure of MIL-53(Fe) is in CAC/MIL-53(Fe).

1-3. SEM

The surface texture features and morphological elements of the prepared samples were investigated using SEM images. Fig. 3 shows the SEM images of the produced samples. On the surface of MIL-53(Fe), there are entirely crystalline spherical particles as well as a tiny number of sheet-like particles (Fig. 3(a) and (b)). The diameter of the spherical particles is approximately 300-600 nm [41]. On the other hand, as mentioned in the XRD analysis, the surface morphology of CAC also shows its amorphous structure (Fig. 3(c) and (d)). As shown in Fig. 3((e) and (f)), due to the high content of CAC in the composite sample, the MOF structures are not seen in the surface texture of the sample, and the presence of large amounts of CAC is evident. This high loading amount of CAC is also considered a substrate for the growth of MOF structures.

1-4. EDX

The EDX spectra and point mapping micrographs, also the weight percentages of the various components present on the adsorbent surface of the composite as mentioned above, are shown in Fig. 4. These images demonstrate that the elements of carbon (65.92%), oxygen (31.28%), and iron (2.7%) are present in various weight percentages on the surface of CAC/MIL-53(Fe) species. Moreover, the point micrographs of this sample indicate that different components are dispersed correctly on the surface of CAC/MIL-53(Fe).

2. Removal Studies

2-1. Effect of Adsorbent Dosage

The dosage of the adsorbent is crucial in influencing the amount

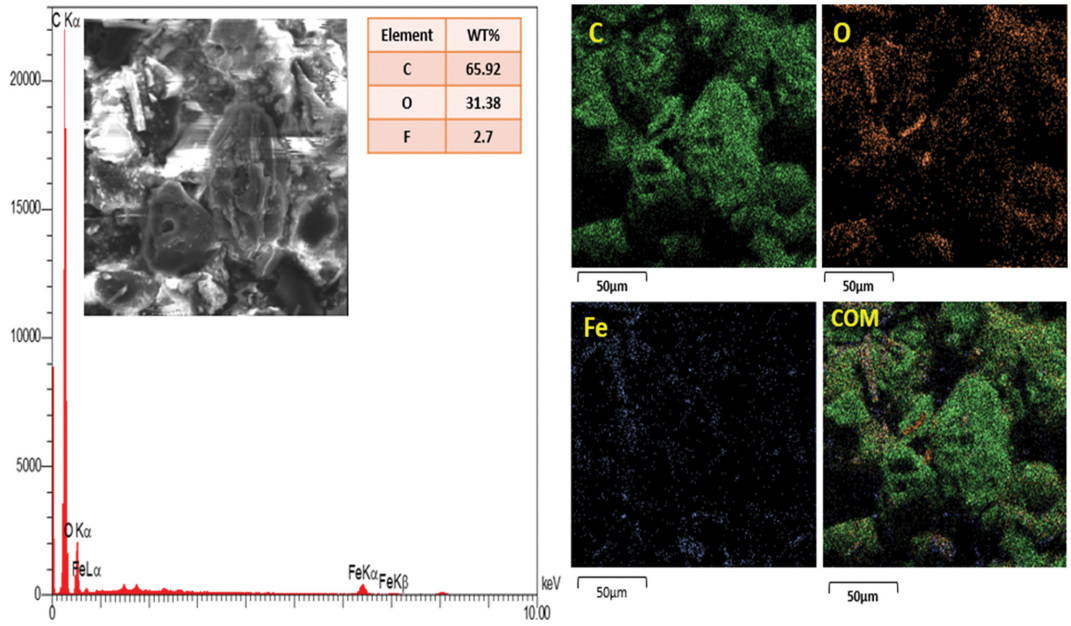

Fig. 4. EDX-dot mapping and surface chemical analysis of the CAC/MIL-53(Fe).

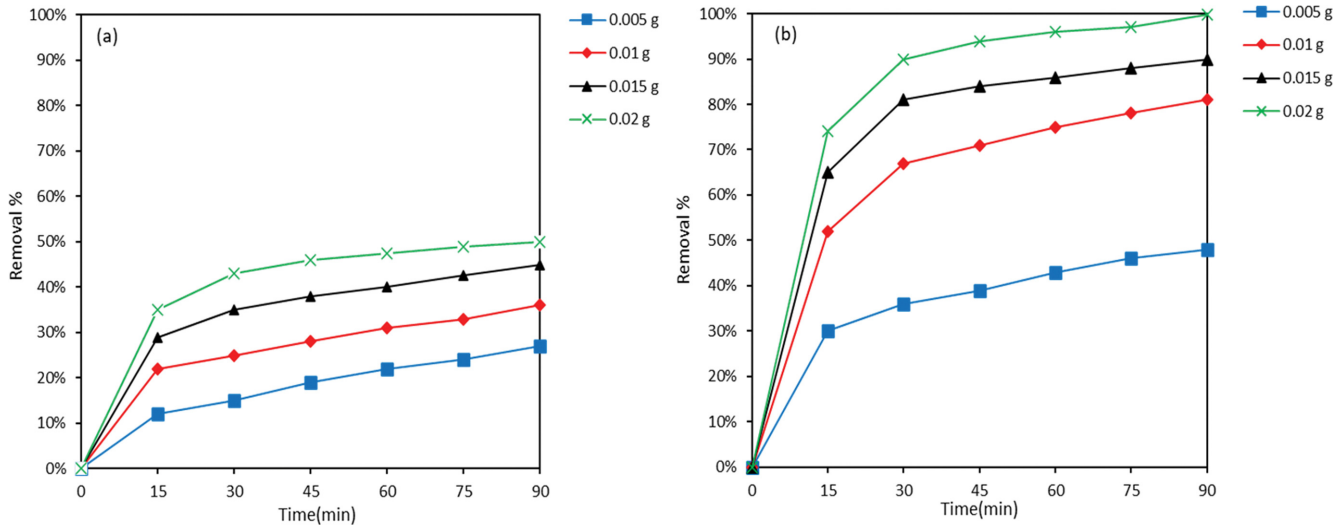

Fig. 5. Effect of adsorbent dosage on dye removal (a) CAC, and (b) CAC/MIL-53(Fe) (T: 25 °C, pH=3, and dye: 20 mg/L).

of dye adsorption on the adsorbent and the cost of pollution removal processes [42]. Fig. 5 shows dye removal in 100 mL of dye solution (DR23) at a concentration of 20 mg/L with pH 3 for 90 min at room temperature using various quantities of adsorbent (0.005, 0.01, 0.015, and 0.02 g). According to findings, dye removal increased by CAC from 27% to 50% and from 48% to 99.9% by CAC/MIL-53(Fe) when the adsorbent dosage was increased. This increase in the removal of dye (%) is attributed to more active sites being available, a larger surface area, and massive radical production, which may be removed by impact with dye molecules at higher adsorbent dosages [43]. On the other hand, the amount of DR23 adsorbed at equilibrium (q_e, mg/g) decreased with increasing adsorbent dosage due to a gap in the flow of a solute concentration gradient among the solution and the adsorbent surface [44]. According to the results, 0.02 g was considered the optimal adsorbent dosage for dye removal.

2-2. Effect of Initial Dye Concentration

The initial dye concentration has a significant effect on the adsorbent performance due to the direct relationship between the dye concentration and the accessible sites on the adsorbent surface. In general, with increased initial dye concentration, the percentage of dye removal decreases, which might be due to saturation of adsorption sites on the adsorbent surface [45]. The influence of the initial dye concentration on adsorption performance is shown in Fig. 6. Various dye concentrations (20, 30, 40, and 50 mg/L) were examined by adjusting at pH=3 and the optimal adsorbent dosage (0.02 g) at room temperature for 90 min. It is observed that with increasing the amount of dye concentration, the dye removal decreases. As shown in Fig. 5, the dye removal was reduced from 50% to 30% and 99.9% and 70% using CAC and CAC/MIL-53(Fe), respectively. Additionally, increasing the initial dye concentration enhanced the adsorption capacity owing to the strong stimulant force for mass transfer [45].

2-3. Effect of Solution pH

The value of pH is one of the important parameters due to the influence on the surface charge and the degree of ionization of sol-

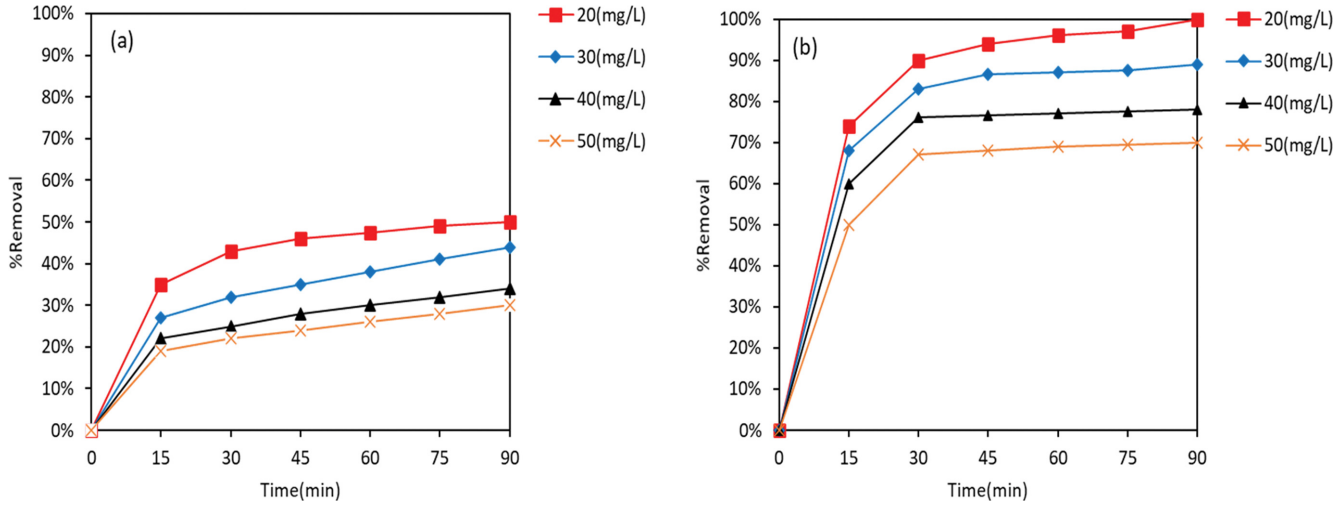

Fig. 6. Effect of initial pollutant concentration on dye adsorption (a) CAC, and (b) CAC/MIL-53(Fe) (pH=3, adsorbent: 0.02 g, and T: 25 °C).

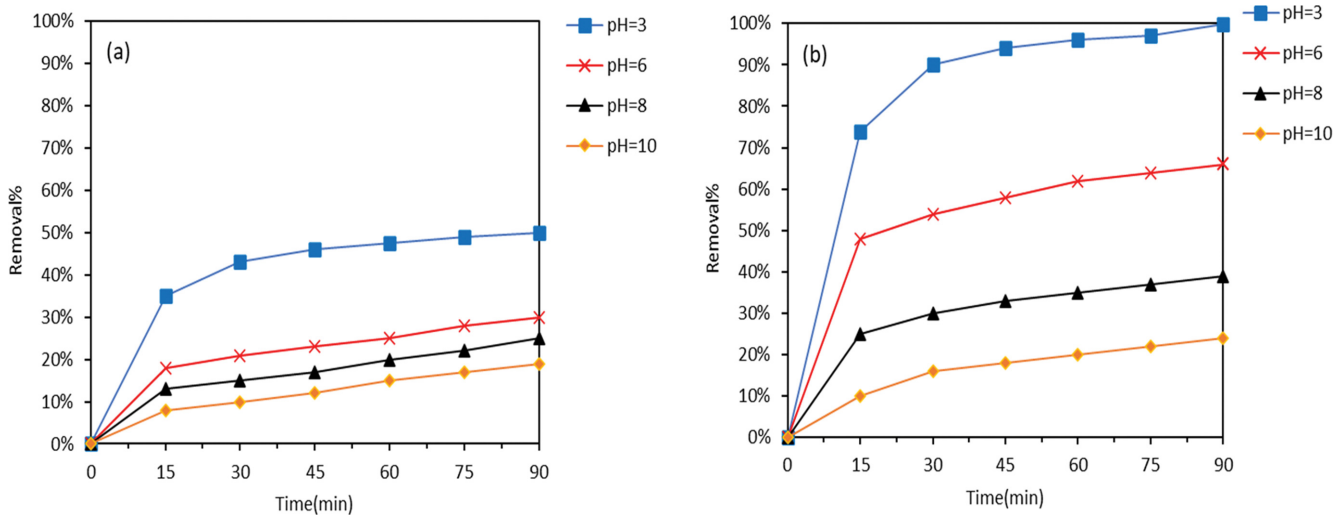

Fig. 7. Effects of the solution pH on dye adsorption (a) CAC, and (b) CAC/MIL-53(Fe) (dye: 20 mg/L, adsorbent: 0.02 g, and T: 25 °C).

ute components. Changes in the initial pH value are connected to changes in the adsorbent surface and dye chemistry, which may either increase or decrease the rate of dye adsorption [46]. To determine the influence of pH on the adsorbent, a dye solution (20 mg/L) was tested at room temperature for 90 min with varying pH values (3, 6, 8, and 10) using an ideal adsorbent dose (20 mg). According to Fig. 7, the amount of dye removal decreases with increasing the pH. Dye removal decreased from 50% to 19% when CAC was used, and from 99.9% to 24% when CAC/MIL-53(Fe) was used. Indeed, since DR23 is an anionic dye, the adsorption capacity decreases with the increasing pH of the solution. At higher pH values, the adsorbent surface becomes negatively charged as functional groups such as hydroxyl and amino are ionized, resulting in strong electrostatic repulsion between the negatively charged adsorbent surface and the negatively charged anionic pollutant molecules. As the pH of the solution decreases, the number of positively charged sites rises on the adsorbent surface. The site has a positive charge on the adsorbent due to electrostatic attraction tends to adsorb anionic contaminants. As a result, acidic pH (pH=3) is optimal.

2-4. Effect of Contact Time

When contaminants are removed from water and wastewater by adsorption at a certain temperature and pH, the contact time is critical between the adsorbent and the adsorbate species. The adsorbent effectiveness in wastewater treatment is measured by fast adsorption of pollutant (dye) and the formation of equilibrium in a short amount of time. Furthermore, one of the variables influencing the formation of surface charges at the solid-liquid interface is contact time [47]. Therefore, the effect of contact time was investigated by keeping the adsorbent dosage (0.02 g), the dye concentration (20 mg/L), pH=3, at room temperature for 1 to 90 min. It was observed that in the first 15 min of velocity, the adsorption was high, and after 30 min the adsorption process slowed, stabilized and saturated (Fig. 8). This decrease in adsorption over time is due to the accumulation of adsorption sites by dye ions, reduction in the adsorbent overall surface area, as well as an increase in the diffusion path [48].

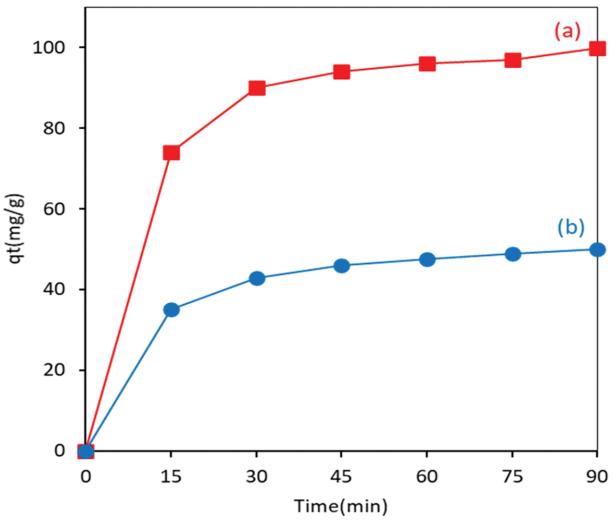

Fig. 8. Effect of contact time on dye adsorption (a) CAC/MIL-53(Fe), and (b) CAC, (pH=3, dye: 20 mg/L, adsorbent: 0.02 g, and T: 25 °C).

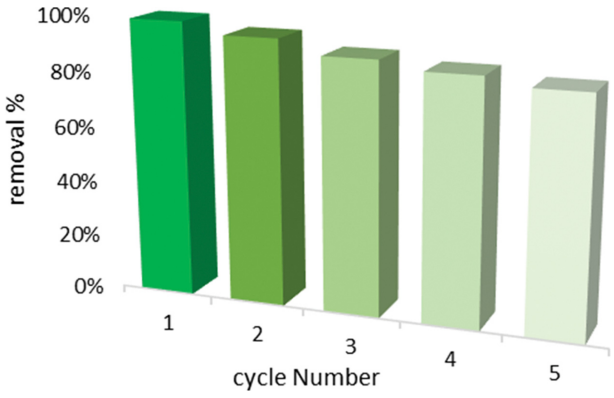

Fig. 9. The reusability of CAC/MIL-53(Fe) composite for removal of DR23.

2-5. Reusability and Stability

The reusability and stability of the composite in the environment to remove pollutants were studied with scientific assessment and the use of adsorbents produced on a large scale. This was repeated five times in a row under ideal conditions (pH=3, dosage=0.02 g, and dye concentration=20 mg/L at room temperature) circumstances using a volume of 100 mL of dye solution. After 90 min, the treated effluent was collected, and the adsorbent was separated by centrifugation into 100 mL. For 60 min, the adsorbent was washed with 10 mL of water/ethanol (0.5 : 0.5) solution. It was then dried for 1 h in an oven at 80 °C. This procedure was repeated using the acquired adsorbent. After five repetitions, the quantity of dye removed was reduced by 15% (Fig. 9).

3. Adsorption Modeling

3-1. Adsorption Isotherms

The efficient use of the adsorption process demands study based on several adsorption isotherm models [49]. The adsorption isotherms describe how the adsorbent interacts with the adsorbate. As a result, the utilization of adsorbents is critical in optimization. The connection between equilibrium data and theoretical equations is essential for developing and operating adsorption systems. The adsorbent interacts with the adsorbate, yielding an adsorption capacity value. The surface phase can be monolayer or multilayer. Equilibrium adsorption isotherms may represent adsorption capacity with particular constants, indicating surface characteristics and adsorbent affinity. The adsorption isotherm is significant in both theoretical and practical terms. The features derived from various models offer critical information about adsorption, surface qualities, and adsorbent affinity. The most frequently used adsorption models for single-solution systems, the Langmuir, and Freundlich models, are among the isotherm equations accessible to study equilibrium isotherm data. The adsorption isotherm displays the relation among the amount of dye adsorbed, the size of the particles, and the temperature [50,51].

The Langmuir isotherm implies that the adsorbent surface is entirely uniform. Each active site of the adsorbent can only adsorb one pollutant molecule, resulting in one-molecule thick adsorbed layers [52]. The Langmuir non-linear and linear models are as follows, Eq. (3) and (4) [53]:

$$q_e = \frac{C_e \cdot K_L \cdot Q_{max}}{1 + K_L C_e} \quad (3)$$

$$\frac{C_e}{q_e} = \frac{1}{k_L \cdot Q_{max}} + \frac{C_e}{Q_{max}} \quad (4)$$

where C_e represents the dye concentration at equilibrium (mg/L). The quantity of dye adsorbed at equilibrium time (mg/g) is represented by q_e. The Langmuir isotherm constant (L/mg) is represented by K_L, and the maximum adsorption capacity (mg/g) is represented by Q_{max} [54].

Furthermore, the Freundlich equation assumes that contaminants are adsorbed in heterogeneous surfaces. The non-linear and linear forms of this model are described by Eqs. (5) and (6) [55]:

$$q_e = k_F C_e^{1/n} \quad (5)$$

$$\log q_e = \log K_F + \frac{1}{n} \log C_e \quad (6)$$

The adsorption intensity and capacity at unit concentration are represented by 1/n and k_F, respectively. Furthermore, isotherms are represented by 1/n values; if (1/n=0), the isotherm is irreversible; (0<1/n<1) is favorable; and (1/n>1) is unfavorable [56-58]:

Fig. 10(a) shows the Langmuir isotherm applicability to dye adsorption on CAC/MIL-53(Fe) using a linear plot of C_e/q_e vs. C_e, and Fig. 10(b) depicts a graph of $\log q_e$ vs. $\log C_e$ for the Freundlich linear model. Fig. 10(c) shows the non-linear isotherm models in the plot of C_e vs. q_e. Also, the constants of linear and non-linear models are presented in Tables 1 and 2.

According to Tables 1 and 2, the Langmuir model provides the highest R^2 values of 0.9855 calculated by a linear model and 0.9294 by non-linear model, which is better than the Freundlich model. Also, the maximum adsorption capacity ($Q_{max, linear}$=196 and $Q_{max, nonlinear}$= 172 mg/g) calculated from the Langmuir equation is close to the maximum experimental adsorption capacity ($q_{e, (exp)}$=192 mg/g). So, according to the results obtained from the linear and nonlin-

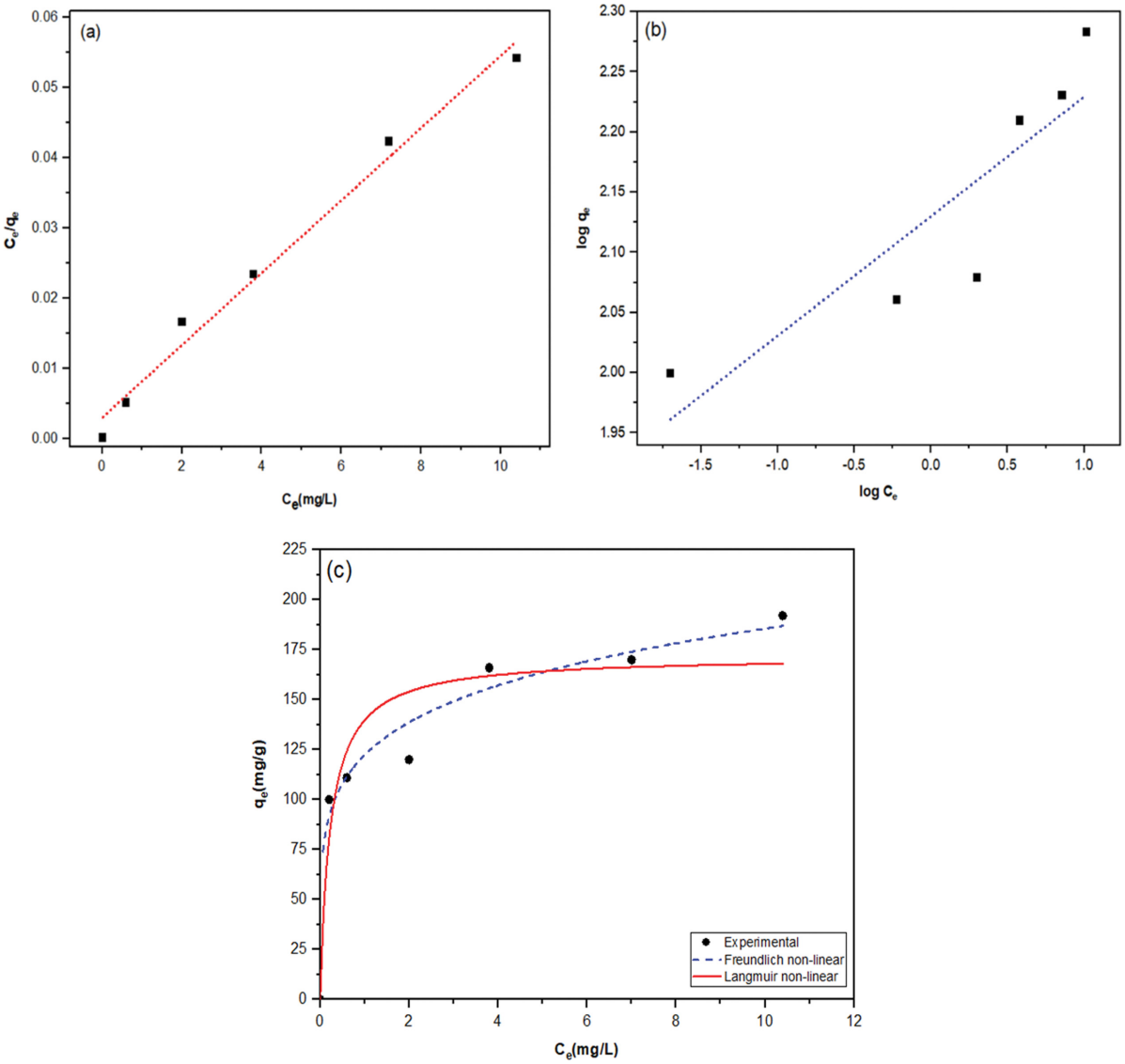

Fig. 10. Isotherm models of DR23 adsorption onto CAC/MIL-53 (a) the Langmuir linear model, (b) the Freundlich linear model, and (c) the Langmuir and Freundlich non-linear models.

Table 1. Constants of linear isotherm models for dye adsorption onto CAC/MIL-53(Fe) at different adsorbent dosages (100 mL solution, T: 25 °C, pH=3, and 20 mg/L)

Isotherm	Parameter	Adsorbents
		CAC/MIL-53(Fe)
Langmuir (Linear form)	Q_{max}	196
$\frac{C_e}{q_e}=\frac{1}{k_L \cdot Q_{max}}+\frac{C_e}{Q_{max}}$	K_L	0.6078
	R^2	0.9855
Freundlich (Linear form)	1/n	0.099
$\log q_e=\log K_F+\frac{1}{n}\log C_e$	K_F	134.896
	R^2	0.7837

Table 2. Constants of non-linear isotherm models for dye adsorption onto CAC/MIL-53(Fe) at different adsorbent dosages (100 mL solution, T: 25 °C, pH=3, and dye: 20 mg/L)

Isotherm	Parameter	Adsorbents
		CAC/MIL-53(Fe)
Langmuir (Non-linear form)	Q_{max}	172
$q_e=\frac{C_e \cdot K_L \cdot Q_{max}}{1+K_L C_e}$	K_L	4.368
	R^2	0.9294
Freundlich (Non-linear form)	1/n	0.18098
$q_e=K_F C_e^{1/n}$	K_F	142.37
	R^2	0.9149

ear models, the Langmuir model shows a better agreement with the experimental data. This means that in the composite, the adsorption of dyes occurs in some homogeneous regions, and the adsorption of a single layer of dyes takes place on the composite surface. Besides, due to the K_L value, the R_L value ($0<R_L<1$) indicates that the adsorption process is favorable.

3-2. Adsorption Kinetics

Adsorption kinetics offers information regarding the adsorption mechanism. Understanding the adsorption process speed is essential for optimizing the parameter design. Adsorption processes are often described using pseudo-first-order, pseudo-second-order, and intraparticle diffusion kinetic models [59]:

The non-linear and linear form of the pseudo-first-order model is generally expressed as Eq. (8) and (9) [60,61]:

$$q_t=q_e(1-e^{(-k_1 \cdot t)}) \tag{7}$$

$$\log(q_e-q_t)=\log(q)-\frac{k_1 \cdot t}{2.303} \tag{8}$$

The adsorption capacity at time t and equilibrium (mg/g) is represented by q_t and q_e, respectively. The pseudo-first-order model adsorption rate constant (1/min) is denoted by k_1, and the contact time by t (min). Fig. 11(a) shows linear graphs of $\log(q_e-q_t)$ vs. time (t) and Fig. 11(b) shows non-linear graphs of q_t vs. time (t). Table 3 also includes the values $q_{e(cal)}$, R^2, and k_1.

Adsorption kinetics can be explained by the pseudo-second-order model. The non-linear and linear equations of this model are shown by the Eqs. (9) and (10) [62,63]:

$$q_t=\frac{k_2 \cdot q_e^2 \cdot t}{1+k_2 \cdot q_e \cdot t} \tag{9}$$

$$\frac{t}{q_t}=\frac{1}{k_2 q^2}+\frac{t}{q_e} \tag{10}$$

k_2 (g/mg min) is the rate constant for the pseudo-second-order adsorption model. Fig. 12(a) shows linear graphs of t/q_t vs. time (t) and Fig. 12(b) shows non-linear graphs of q_t vs. time (t). Table 4 lists the values for $q_{e(cal)}$, R^2, and k_2.

Intraparticle diffusion kinetics shows the rate of velocity and transfer of solute molecules from the aqueous phase to the surface of solid particles (adsorbents) and then the diffusion of solute molecules into the pores in the adsorption process, which is predicted

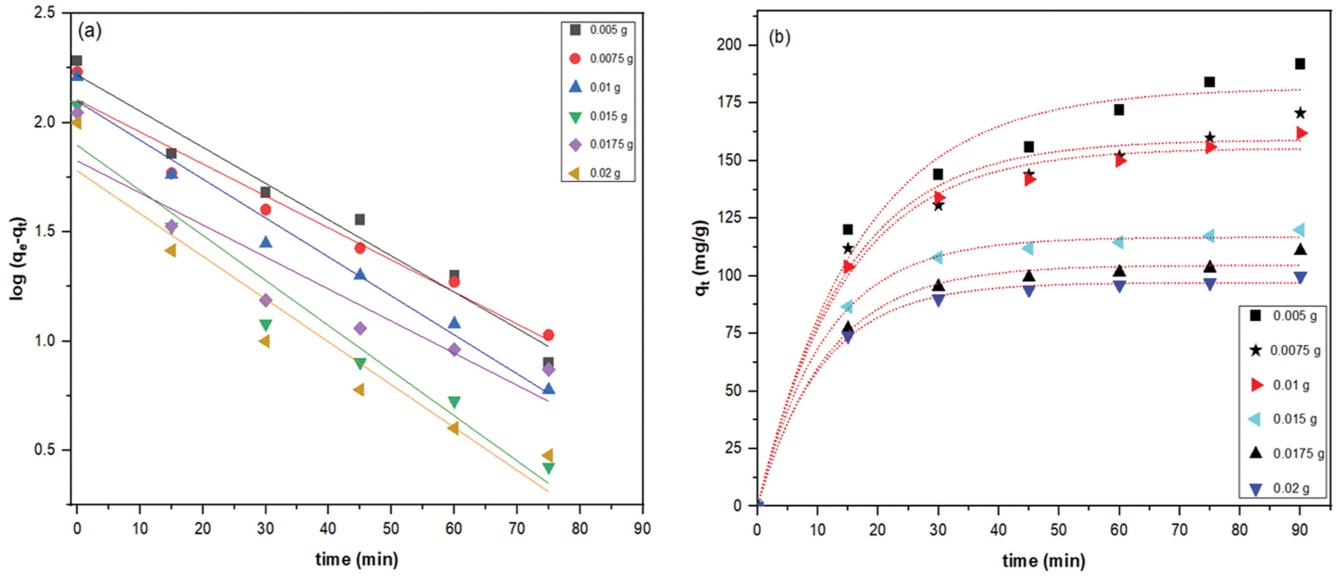

Fig. 11. Pseudo-first-order kinetics (a) linear model, and (b) non-linear model.

Table 3. Pseudo-first-order kinetic constants for dye adsorption onto CAC/MIL-53(Fe) at different adsorbent dosages (pH=3, dye: 20 mg/L, and T: 25 °C)

Adsorbent	Dosage (g)	$q_{e(exp)}$	Pseudo-first-order (linear form)				Pseudo-first-order (non-linear form)			
			$q_{e(cal)}$	k_2	R^2	χ^2	$q_{e(cal)}$	k_2	R^2	χ^2
CAC/MOF	0.005	192	165	0.0382298	0.9672	4.42	181	0.06	0.97865	0.67
	0.0075	171	127	0.0336238	0.95831	15.24	160	0.071	0.97084	0.76
	0.01	162	125	0.0409934	0.97405	10.95	155	0.068	0.98391	0.32
	0.015	120	79	0.0474418	0.94814	21.28	116	0.088	0.9887	0.14
	0.0175	111	67	0.0338541	0.87056	28.90	104	0.8554	0.98345	0.47
	0.02	100	62	0.0504357	0.91919	23.29	95	0.9311	0.9879	0.26

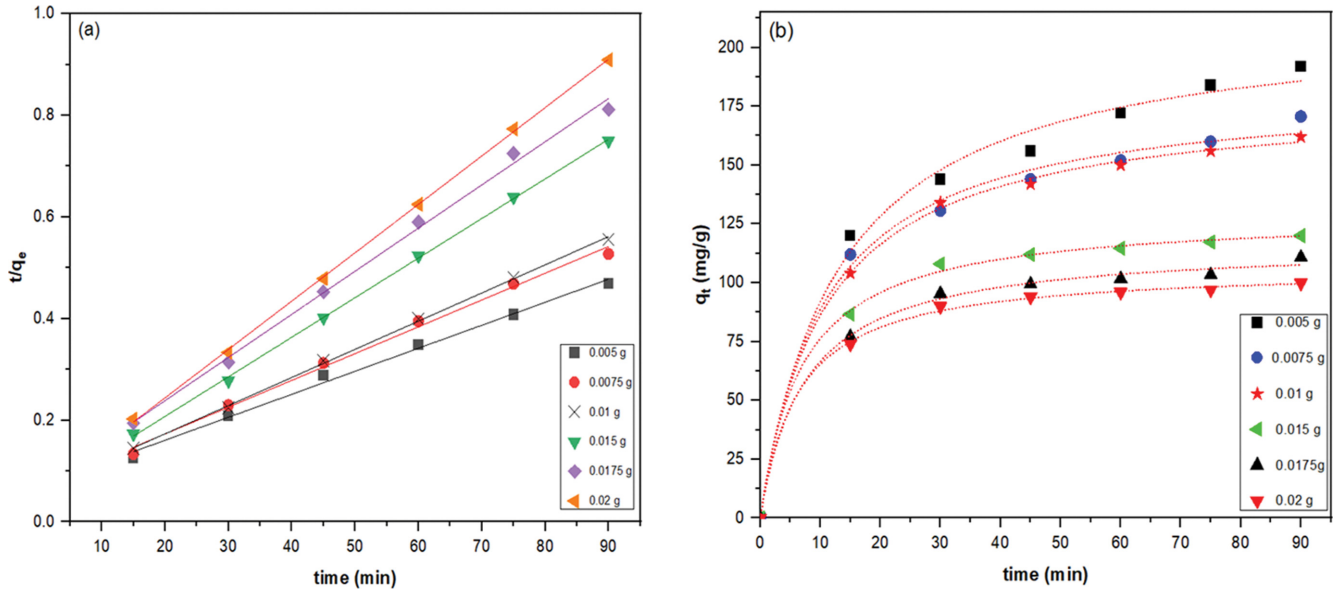

Fig. 12. Pseudo-second-order kinetics (a) linear model, and (b) non-linear model.

Table 4. Pseudo-second-order kinetic constants for dye adsorption onto CAC/MIL-53(Fe) at different adsorbent dosages (pH=3, dye: 20 mg/L, and T: 25 °C)

Adsorbent	Dosage (g)	$q_{e(exp)}$	Pseudo-second-order (linear form)				Pseudo-second-order (non-linear form)			
			$q_{e(cal)}$	k_2	R^2	χ^2	$q_{e(cal)}$	k_2	R^2	χ^2
CAC/MOF	0.005	192	222	0.00029	0.9936	4.05	212	3.56	0.99268	1.89
	0.0075	171	189	0.00041	0.9945	1.71	182	5.15	0.99420	0.66
	0.01	162	182	0.00021	0.9990	2.20	175	5.21	0.99901	0.97
	0.015	120	128	0.00117	0.9995	0.50	129	0.00111	0.9987	0.63
	0.0175	111	118	0.00105	0.9963	0.42	116	0.00115	0.9975	0.22
	0.02	100	105	0.00167	0.9997	0.24	104	0.00167	0.99908	0.15

to be slow. Eq. (11) is used to investigate the concept of intraparticle diffusion [64,65]:

$$q_t = k_p t^{1/2} + I \tag{11}$$

where k_p is the rate constant of intraparticle diffusion. To demonstrate the model applicability, linear graphs of q_t vs. $t^{1/2}$ for dye adsorption on CAC/MIL-53(Fe) are shown in Fig. 13. The k_p, I, and (R^2) for these plots were computed and listed in Table 5.

Furthermore, Chi-square (χ^2) was utilized as a fitness test by comparing experimental and model-calculated equilibrium adsorption data. The value of (χ^2) is calculated by the Eq. (12) [66].

$$\chi^2 = \frac{\Sigma(q_{e(exp)} - q_{e(cal)})}{q_{e(cal)}} \tag{12}$$

where $q_{e(exp)}$ and $q_{e(cal)}$ (mg/g), are the adsorption capacity at equilibrium experimental condition and model-calculated adsorption capacity, respectively. A low value of (χ^2) shows that the model results are consistent with the experimental value.

Table 5. Intraparticle diffusion kinetics model constants for dye adsorption onto CAC/MIL-53(Fe) at different adsorbent dosages (pH=3, dye: 20 mg/L, and T: 25 °C)

Adsorbent	Dosage (g)	$q_{e(exp)}$	Intraparticle diffusion				
			$q_{e(cal)}$	K_p	I	R^2	χ^2
CAC/MOF	0.0050	192	179	11.872	66.333	0.9863	0.94
	0.0075	171	156	9.114	69.174	0.9852	1.44
	0.0100	162	151	8.6833	68.629	0.9288	0.80
	0.0150	120	109	4.348	67.385	0.8521	1.11
	0.0175	111	96	4.1883	56.724	0.8794	2.34
	0.0200	100	87	3.0327	58.47	0.8368	1.94

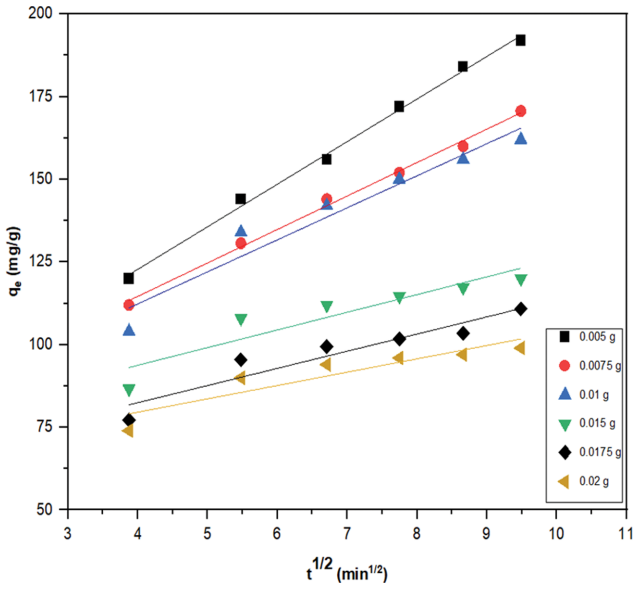

Fig. 13. Intraparticle diffusion kinetics model.

For the best fit kinetic model, three parameters were investigated: (i) The maximum correlation coefficient values (R^2), (ii) the minimum value of χ^2, and (c) the $q_{e(exp)}$ values that should reasonably match with the $q_{e(cal)}$ values.

According to the results obtained from the three kinetics, the adsorption kinetic follows pseudo-second-order because the linear and non-linear pseudo-second-order model shows the highest R^2 (linear=0.9997, non-linear=0.99908), the lowest χ^2 linear=0.24, non-linear=0.15, and the correlation between $q_{e(exp)}$ and $q_{e(cal)}$.

CONCLUSION

CAC/MIL-53(Fe) composite was successfully synthesized with a mass ratio of 1 : 0.3 via the solvothermal method. Crystal structures grew immediately on the CAC surface after the MOF was synthesized in the presence of CAC. The manufacturer of the MOF component considerably expanded the dye that the CAC could adsorb, making it acceptable for dye wastewater cleanup operations. The adsorption process parameters (the different adsorbent dosages, initial dye concentration, the pH of the solution and contact time) and reusability were investigated. Under optimal conditions (pH=3, 20 mg/L, 0.02 g, 90 min, and 25 °C), the dye removal and the maximum adsorption capacity of the CAC/MIL-53(Fe) composite were 99.9% and 100 mg/g, respectively. Dye removal followed the Langmuir isotherm and the pseudo-second-order kinetic. Ultimately, the reusability of the CAC/MIL-53(Fe) composite in removing the DR23 after five cycles was satisfactory.

REFERENCES

1. D. Asefi, N. M. Mahmoodi and M. Arami, *Colloids Surf. A: Physicochem. Eng. Asp.*, **355**, 183 (2010).
2. N. M. Mahmoodi and M. Arami, *J. Appl. Polym. Sci.*, **109**, 4043 (2008).
3. N. M. Mahmoodi, *J. Environ. Eng.*, **139**, 1368 (2013).
4. N. M. Mahmoodi, M. Arami, N. Y. Limaee, K. Gharanjig and F. D. Ardejani, *Colloids Surf. A: Physicochem. Eng. Asp.*, **290**, 125 (2006).
5. S. Davarpanah, N. M. Mahmoodi, M. Arami, H. Bahrami and F. Mazaheri, *Appl. Surf. Sci.*, **255**, 4171 (2009).
6. N. M. Mahmoodi, *Water, Air, Soil Pollut.*, **224**, 1419 (2013).
7. N. M. Mahmoodi and M. Arabloo, *J. Abdi, Water Res.*, **67**, 216 (2014).
8. N. M. Mahmoodi, N. Y. Limaee, M. Arami, S. Borhany and M. Mohammad-Taheri, *J. Photochem. Photobiol. A: Chem.*, **189**, 1 (2007).
9. A. Bhatnagar, W. Hogland, M. Marques and M. Sillanpää, *Chem. Eng. J.*, **219**, 499 (2013).
10. M. Hasanzadeh, A. Simchi and H. S. Far, *J. Ind. Eng. Chem.*, **81**, 405 (2020).
11. K. L. B. Solis, Y.-H. Kwon, M.-H. Kim, H.-R. An, C. Jeon and Y. Hong, *Chemosphere*, **238**, 124656 (2020).
12. O. Yaghi and G. Li, *Angew. Chem. Int. Ed. Engl.*, **34**, 207 (1995).
13. G. Férey, C. Mellot-Draznieks, C. Serre, F. Millange, J. Dutour, S. Surblé and I. Margiolaki, *Science*, **309**, 2040 (2005).
14. O. M. Yaghi, M. O'Keeffe, N. W. Ockwig, H. K. Chae, M. Eddaoudi and J. Kim, *Nature*, **423**, 705 (2003).
15. O. K. Farha, A. Ö. Yazaydın, I. Eryazici, C. D. Malliakas, B. G. Hauser, M. G. Kanatzidis, S. T. Nguyen, R. Q. Snurr and J. T. Hupp, *Nat. Chem.*, **2**, 944 (2010).
16. A. G. Wong-Foy, A. J. Matzger and O. M. Yaghi, *J. Am. Chem. Soc.*, **128**, 3494 (2006).
17. S. K. Bhardwaj, N. Bhardwaj, G. C. Mohanta, P. Kumar, A. L. Sharma, K.-H. Kim and A. Deep, *ACS Appl. Mater. Interface*, **7**, 26124 (2015).
18. Z. Hasan and S. H. Jhung, *J. Hazard. Mater.*, **283**, 329 (2015).
19. N. A. Khan, Z. Hasan and S. H. Jhung, *J. Hazard. Mater.*, **244**, 444

(2013).
20. J. Liu, L. Chen, H. Cui, J. Zhang, L. Zhang and C.-Y. Su, *Chem. Soc. Rev.*, **43**, 6011 (2014).
21. P. Ramaswamy, N. E. Wong and G. K. Shimizu, *Chem. Soc. Rev.*, **43**, 5913 (2014).
22. T. Zhang and W. Lin, *Chem. Soc. Rev.*, **43**, 5982 (2014).
23. N. M. Mahmoodi, *Desalin. Water Treat.*, **53**, 84 (2015).
24. P. Horcajada, T. Chalati, C. Serre, B. Gillet, C. Sebrie, T. Baati, J. F. Eubank, D. Heurtaux, P. Clayette and C. Kreuz, *Nat. Mater.*, **9**, 172 (2010).
25. B. P. McGrail, P. K. Thallapally, J. Blanchard, S. K. Nune, J. J. Jenks and L. X. Dang, *Nano Energy*, **2**, 845 (2013).
26. Y. Chen and S. Ma, *Dalton Trans.*, **45**, 9744 (2016).
27. W. Xiong, G. Zeng, Z. Yang, Y. Zhou, C. Zhang, M. Cheng, Y. Liu, L. Hu, J. Wan and C. Zhou, *Sci. Total Environ.*, **627**, 235 (2018).
28. S. B. Bagherzadeh, M. Kazemeini and N. M. Mahmoodi, *J. Mol. Liq.*, **301**, 112427 (2020).
29. Z. Yang, X. Xu, X. Liang, C. Lei, Y. Wei, P. He, B. Lv, H. Ma and Z. Lei, *Appl. Catal., B: Environ.*, **198**, 112 (2016).
30. T. Van Tran, V. Dai Cao, V. H. Nguyen, B. N. Hoang, D.-V. N. Vo, T. D. Nguyen and L. G. Bach, *J. Environ. Chem. Eng.*, **8**, 102902 (2020).
31. M. Abniki, A. Moghimi and F. Azizinejad, *J. Serb. Chem. Soc.*, **85**, 1223 (2020).
32. X. Feng, H. Chen and F. Jiang, *J. Colloid Interface Sci.*, **494**, 32 (2017).
33. P. Horcajada, C. Serre, G. Maurin, N. A. Ramsahye, F. Balas, M. Vallet-Regi, M. Sebban, F. Taulelle and G. Férey, *J. Am. Chem. Soc.*, **130**, 6774 (2008).
34. C. Zhang, L. Ai and J. Jiang, *J. Mater. Chem. A*, **3**, 3074 (2015).
35. P. Llewellyn, P. Horcajada, G. Maurin, T. Devic, N. Rosenbach, S. Bourrelly, C. Serre, D. Vincent, S. Loera-Serna and Y. Filinchuk, *J. Mater. Chem. A*, **131**, 13002 (2009).
36. H. Li, F. Zheng, J. Wang, J. Zhou, X. Huang, L. Chen, P. Hu, J.-m. Gao, Q. Zhen and S. Bashir, *Chem. Eng. J.*, **390**, 124513 (2020).
37. M. Uchimiya, L. H. Wartelle, K. T. Klasson, C. A. Fortier and I. M. Lima, *J. Agric. Food. Chem.*, **59**, 2501 (2011).
38. M. T. Sikder, T. Kikuchi, J. Suzuki, T. Hosokawa, T. Saito and M. Kurasaki, *Sep. Sci. Technol.*, **48**, 587 (2013).
39. R. Shahrokhi-Shahraki, C. Benally, M. G. El-Din and J. Park, *Chemosphere*, **264**, 128455 (2021).
40. D. Kołodyńska, J. Krukowska and P. Thomas, *Chem. Eng. J.*, **307**, 353 (2017).
41. J.-J. Du, Y.-P. Yuan, J.-X. Sun, F.-M. Peng, X. Jiang, L.-G. Qiu, A.-J. Xie, Y.-H. Shen and J.-F. Zhu, *J. Hazard. Mater.*, **190**, 945 (2011).
42. G. Crini and P.-M. Badot, *Prog. Polym. Sci.*, **33**, 399 (2008).
43. S. Chen, J. Zhang, C. Zhang, Q. Yue, Y. Li and C. Li, *Desalination*, **252**, 149 (2010).
44. S. Liu, Y. Ding, P. Li, K. Diao, X. Tan, F. Lei, Y. Zhan, Q. Li, B. Huang and Z. Huang, *Chem. Eng. J.*, **248**, 135 (2014).
45. M. T. Yagub, T. K. Sen, S. Afroze and H. M. Ang, *Adv. Colloid Interface Sci.*, **209**, 172 (2014).
46. K. Foo and B. H. Hameed, *Desalin. Water Treat.*, **19**, 255 (2010).
47. S. Khattri and M. Singh, *J. Hazard. Mater.*, **167**, 1089 (2009).
48. A. Mittal, J. Mittal, A. Malviya and V. Gupta, *J. Colloid Interface Sci.*, **340**, 16 (2009).
49. A. Mittal, L. Kurup and J. Mittal, *J. Hazard. Mater.*, **146**, 243 (2007).
50. N. M. Mahmoodi, *J. Mol. Catal. A: Chem.*, **366**, 254 (2013).
51. N. M. Mahmoodi, *J. Environ. Eng.*, **139**(11), 1382 (2013).
52. N. M. Mahmoodi, *J. Taiwan Inst. Chem. Eng.*, **45**, 2008 (2014).
53. N. M. Mahmoodi, M. Taghizadeh and A. Taghizadeh, *J. Mol. Liq.*, **277**, 310 (2019).
54. N. M. Mahmoodi, B. Hayati and M. Arami, *J. Chem. Eng. Data*, **55**, 4638 (2010).
55. A. Kausar, G. MacKinnon, A. Alharthi, J. Hargreaves, H. N. Bhatti and M. Iqbal, *J. Mol. Liq.*, **257**, 164 (2018).
56. N. M. Mahmoodi, M. Oveisi, A. Taghizadeh and M. Taghizadeh, *Carbohydr. Polym.*, **227**, 115364 (2020).
57. R. Foroutan, R. Mohammadi and B. Ramavandi, *Environ. Sci. Pollut. Res.*, **26**, 19523 (2019).
58. B. Hayati and N. M. Mahmoodi, *Desalin. Water Treat.*, **47**, 322 (2012).
59. N. M. Mahmoodi and F. Najafi, *Micropor. Mesopor. Mater.*, **156**, 153 (2012).
60. M. Abniki and A. Moghimi, *Micro Nano Lett.*, **16**, 455 (2021).
61. A. Roghanizad, M. K. Abdolmaleki, S. M. Ghoreishi and M. Dinari, *J. Mol. Liq.*, **300**, 112367 (2020).
62. A. Moghimi and M. Abniki, *Russ. J. Phys. Chem. B.*, **15**, S130 (2021).
63. F. Takmil, H. Esmaeili, S. M. Mousavi and S. A. Hashemi, *Adv. Powder Technol.*, **31**, 3236 (2020).
64. A. El Nemr, *J. Hazard. Mater.*, **161**, 132 (2009).
65. N. M. Mahmoodi and S. Soltani-Gordefaramarzi, *Prog. Color Colorants Coat.*, **9**, 85 (2016).
66. R. Abbas, H. Hami and N. Mahdi, *Int. J. Environ. Sci. Technol.*, **16**, 5439 (2019).